INTERNATIONAL JOURNAL FOR NUMERICAL METHODS IN ENGINEERING
Int. J. Numer. Meth. Engng 2008; **74**:799–826
Published online 30 October 2007 in Wiley InterScience (www.interscience.wiley.com). DOI: 10.1002/nme.2178

On the integration schemes for Drucker–Prager's elastoplastic models based on exponential maps

M. Rezaiee-Pajand*, † and Cyrus Nasirai

Department of Civil Engineering, Ferdowsi University of Mashhad, Mashhad, Iran

SUMMARY

Rate plasticity equations for the case of Drucker–Prager's model in small strain regime are considered. By defining an *augmented* stress vector, the formulations convert the original problem into a quasi-linear differential equation system. Two new exponential mapping schemes for integrating model equations are proposed. In addition, two traditional schemes for solving the dynamical system in an explicit manner are discussed. The two semi-implicit schemes developed pose higher accuracy and better convergency. Error contours are provided for all four methods to display the accuracy of each scheme. In order to compare the results, these contours for the classical *one-step backward Euler* integration method are also displayed. Accuracy and efficiency along with the rate of convergency of the existing and the proposed methods are examined by numerical examples. Copyright © 2007 John Wiley & Sons, Ltd.

Received 3 July 2006; Revised 24 July 2007; Accepted 24 July 2007

KEY WORDS: numerical integration; exponential maps; augmented stress vector; integrating factor; Drucker–Prager

1. INTRODUCTION

A non-linear finite element analysis of structures is usually based on iterative solution of equilibrium equations. Upon these, incremental strain histories are generated. Then updated stresses due to given strains are obtained. The constitutive equations of the material characterize stress as a function of the deformation history. Finally, the equilibrium equations are checked for the updated stress distribution and, if violated, the iteration process continued. One of the important steps in the above procedure is the stress-updating algorithm. The stress-updating procedure requires a large amount of calculations, even for simple plasticity models. A solid three-dimensional model

*Correspondence to: M. Rezaiee-Pajand, Department of Civil Engineering, Ferdowsi University of Mashhad, Mashhad, Iran.
†E-mail: mrpajand@yahoo.com

may have several thousand stress points at which updating stress calculations are required in each load step and in its corrective iterations. Due to the non-linearity of constitutive equations, stress updating may not be performed in an exact manner. This process is normally performed by numerical integration of elastoplastic constitutive equations.

Drucker–Prager's yield criterion is frequently adopted to simulate the behavior of geomaterials. While it is one of the simplest yield functions, it still poses several challenges not encountered in the widely used von-Mises' yield function. One of the simplest and commonly used methods for integration of Drucker–Prager's plasticity model is the *one-step backward Euler* integration method. This scheme is widely used in commercial codes for its simplicity, accuracy and stability. An accurate numerical solution for Drucker–Prager's model was presented by Loret and Prevost [1]. As mentioned there and also investigated in this work, the method is very time consuming and may be used only as a benchmark for more rapid and less accurate numerical methods. Genna and Pandolfi [2] presented a two-step integration scheme for the rate plasticity equations of Drucker–Prager's model with linear mixed hardening. The method was based on a *tangent predictor* and a *non-radial return corrector*. The accuracy of their scheme was not significantly better than that of the *one-step backward Euler* method, but it could handle the singularity point of the yield function.

In the past several years, further attention has been paid to develop new integration techniques based on the internal symmetries of simple constitutive models. If the numerical procedure can take the internal symmetry of the constitutive model into account, the plastic consistency condition is completely satisfied at the end of each time step [3–5]. Auricchio and Beirão da Veiga [6] converted the original non-linear differential problem of von-Mises' plasticity into a dynamical system $\dot{\mathbf{X}} = \mathbb{A}\mathbf{X}$ for an augmented stress vector $\mathbf{X}$. Then they developed a new numerical scheme by employing an exponential map, $\exp(\mathbb{A}_n \Delta t)$, as an approximation to the above system. Artioli *et al.* [7] enhanced this method to obtain a fully consistent algorithm. Finally, further improvements were made to this scheme and consistent methods with a second-order accuracy were developed [8, 9]. Liu [10] investigated the internal symmetry of a constitutive model of Drucker–Prager's type and converted this model into a dynamical system $\dot{\mathbf{X}} = \mathbb{A}\mathbf{X}$ using two separate approaches. The solution of this system was based on exponential maps in an *explicit* manner.

In the present study, Liu's work [10] is explained through introducing new and less complicated parameters and by offering additional numerical tests. In addition, two new stress-updating algorithms are offered in a *semi-implicit* manner with great accuracy and rapid convergency. To completely display the accuracy of all formulations, their iso-error maps are drawn and compared with the contours corresponding to the classical Euler's backward method. Furthermore, to investigate the accuracy and rate of convergency of all schemes, a pointwise strain-controlled load history with different time steps is considered, and the respective error graphs are plotted.

To simplify the descriptive and numerical part of the work, all second-order tensors are considered as 9-component column vectors by ordering the tensor components in a vector format. Owing to the symmetry of second-order tensors, the number of independent components may be reduced to 6. Clearly, the definition of the trace operator and the Euclidean norm must be modified.

2. BASIC MODEL

An associative Drucker–Prager's plasticity model in a small strain domain is adopted. It is supposed that the material behavior is perfectly plastic with no hardening. The total stress and strain, $\boldsymbol{\varepsilon}$ and $\boldsymbol{\sigma}$,

DOI: 10.1002/nme

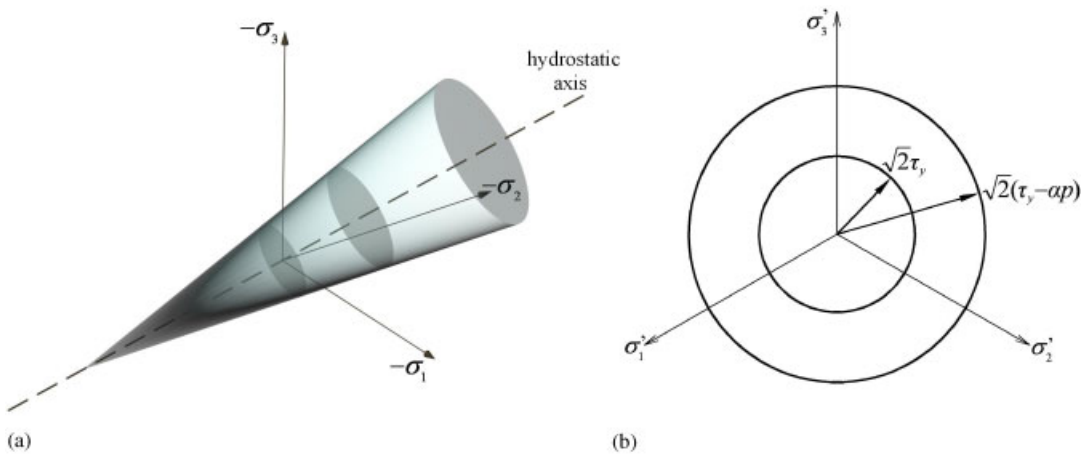

Figure 1. Drucker–Prager's yield surface in: (a) principal stress space and (b) deviatoric planes.

are decomposed into deviatoric and volumetric components as follows:

$$\boldsymbol{\sigma} = \mathbf{s} + p\mathbf{i} \quad \text{with } p = \tfrac{1}{3}\,\mathrm{tr}(\boldsymbol{\sigma}) \tag{1}$$

$$\boldsymbol{\varepsilon} = \mathbf{e} + \tfrac{1}{3}\varepsilon_v \mathbf{i} \quad \text{with } \varepsilon_v = \mathrm{tr}(\boldsymbol{\varepsilon}) \tag{2}$$

where 'tr' indicates the trace operator and $\mathbf{i}$ is the vector corresponding to the second-order identity tensor. $\mathbf{s}$, $\mathbf{e}$, p and ε_v are the deviatoric stress, deviatoric strain, hydrostatic stress and volumetric strain, respectively. The original Drucker–Prager's criterion, formulated in 1952, is a simple modification of the von-Mises' criterion, where the influence of the hydrostatic stress component on the failure is introduced by the inclusion of an additional term

$$f = \sqrt{J_2} + \alpha p - \tau_y = 0 \tag{3}$$

where J_2 is the second invariant of the deviatoric stress tensor. τ_y, the yield stress in pure shear, and α are material parameters which are constant in a perfect plasticity model. These parameters are related to the angle of friction and the cohesion of a geomaterial. These relationships are available in many references, e.g. Chen and Han [11]. Drucker–Prager's criterion defines a cone in the principal stress space as presented in Figure 1(a).

As shown in Figure 1(b), the radius of the yield surface in the π-plane is $\sqrt{2}\tau_y$ and the radius of the yield surface in any other deviatoric plane will be $\sqrt{2}(\tau_y - \alpha p)$. In this figure σ_1', σ_2' and σ_3' are the projections of the principal axes on the deviatoric plane. By rearranging Equation (3), the yield function can be written as

$$F = \tfrac{1}{2}\mathbf{s}^{\mathrm{T}}\mathbf{s} - (\tau_y - \alpha p)^2 = 0, \quad \tau_y - \alpha p > 0 \tag{4}$$

The total strain and volumetric strain increments are considered as the sum of an elastic and a plastic part

$$\dot{\boldsymbol{\varepsilon}} = \dot{\boldsymbol{\varepsilon}}^e + \dot{\boldsymbol{\varepsilon}}^p \tag{5}$$

$$\dot{\varepsilon}_v = \dot{\varepsilon}_v^e + \dot{\varepsilon}_v^p \tag{6}$$

DOI: 10.1002/nme

Note that, in contrast to the von-Mises' criterion, the volumetric component is not treated elastically. The total stress increment for isotropic materials is given by the generalized Hooke's law

$$\dot{\boldsymbol{\sigma}} = 2G\dot{\boldsymbol{\varepsilon}}^e + (K - \tfrac{2}{3}G)\dot{\varepsilon}_v^e \mathbf{i} \tag{7}$$

where G and K are the shear and bulk module, respectively. These two constants with τ_y and α are four material parameters that may be determined by experiments. Using Equations (1) and (7), one obtains

$$\dot{p} = K\dot{\varepsilon}_v^e \tag{8}$$

In an associative flow rule, plastic strain increment is normal to the yield surface and its length is defined by $\dot{\lambda}$ as follows:

$$\dot{\boldsymbol{\varepsilon}}^p = \dot{\lambda}\frac{\partial F}{\partial \boldsymbol{\sigma}} \tag{9}$$

Using Equation (4), the above equation leads to

$$\dot{\boldsymbol{\varepsilon}}^p = \dot{\lambda}\left[\mathbf{s} + \frac{2\alpha}{3}(\tau_y - \alpha p)\mathbf{i}\right] \tag{10}$$

Considering $\mathrm{tr}(\mathbf{s}) = 0$, one obtains

$$\dot{\varepsilon}_v^p = 2\alpha\dot{\lambda}(\tau_y - \alpha p) \tag{11}$$

Substituting Equations (6) and (11) into Equation (8) yields

$$\dot{p} = K\dot{\varepsilon}_v - 2\alpha K\dot{\lambda}(\tau_y - \alpha p) \tag{12}$$

The increment of deviatoric stress, $\dot{\mathbf{s}}$, is obtained by considering the increment of elastic deviatoric strain and the elastic shear modulus as follows:

$$\dot{\mathbf{s}} = 2G\dot{\mathbf{e}}^e = 2G(\dot{\mathbf{e}} - \dot{\mathbf{e}}^p) \tag{13}$$

Using Equations (5) and (2), one obtains the following equation:

$$\dot{\mathbf{e}}^p = \dot{\mathbf{e}}^e - \tfrac{1}{3}\dot{\varepsilon}_v^p \mathbf{i} \tag{14}$$

Substituting Equations (10) and (11) into the above equation yields

$$\dot{\mathbf{e}}^p = \dot{\lambda}\mathbf{s} \tag{15}$$

Finally, using Equations (15) and (13), the following equation is achieved:

$$\dot{\mathbf{s}} = 2G\dot{\mathbf{e}} - 2G\dot{\lambda}\mathbf{s} \tag{16}$$

Equations (12) and (16) are constitutive equations in terms of deviatoric and dilatational components. The Kuhn–Tucker loading–unloading conditions are

$$\dot{\lambda} \geqslant 0, \quad F \leqslant 0, \quad \dot{\lambda}F = 0 \tag{17}$$

The material behaves plastically if $\dot{\lambda} > 0$ and elastically when $\dot{\lambda} = 0$. According to Equation (17) there are two phases: (i) $\dot{\lambda} > 0$ and $F = 0$ or the *ON phase* and (ii) $\dot{\lambda} = 0$ and $F \leqslant 0$ or the *OFF*

DOI: 10.1002/nme

phase. In order to explain the ON–OFF switch, finding a relationship for $\dot{\lambda}$ is necessary. This can be accomplished by combining Equations (12) and (16) with the following consistency condition:

$$\dot{F} = 0 \tag{18}$$

or

$$\mathbf{s}^{\mathrm{T}}\dot{\mathbf{s}} + 2\alpha\dot{p}(\tau_{\mathrm{y}} - \alpha p) = 0 \tag{19}$$

which leads to

$$\dot{\lambda} = \frac{G\mathbf{s}^{\mathrm{T}}\dot{\mathbf{e}} + \alpha K(\tau_{\mathrm{y}} - \alpha p)\dot{\varepsilon}_v}{2H(\tau_{\mathrm{y}} - \alpha p)^2} \tag{20}$$

where H is a material constant defined by

$$H := G + \alpha^2 K \tag{21}$$

Since the denominator of Equation (20) is positive, the following criteria for plastic irreversibility that is based on the Kuhn–Tucker conditions, Equation (17), will be revealed:

$$\begin{aligned} &G\mathbf{s}^{\mathrm{T}}\dot{\mathbf{e}} + \alpha K(\tau_{\mathrm{y}} - \alpha p)\dot{\varepsilon}_v > 0 \quad \text{and} \quad F = 0 \quad \Leftrightarrow \quad \text{ON phase} \\ &G\mathbf{s}^{\mathrm{T}}\dot{\mathbf{e}} + \alpha K(\tau_{\mathrm{y}} - \alpha p)\dot{\varepsilon}_v \leqslant 0 \quad \text{or} \quad F < 0 \quad \Leftrightarrow \quad \text{OFF phase} \end{aligned} \tag{22}$$

3. AUGMENTED DIFFERENTIAL EQUATION SYSTEM (ALGORITHM I)

Liu [10] used the constitutive differential Equations (12) and (16) and converted them into the following dynamical system that could be solved by an exponential map algorithm:

$$\dot{\mathbf{X}} = \mathbb{A}\mathbf{X} \tag{23}$$

where $\mathbf{X}$ is an augmented stress vector with $n + 2$ dimensions and will be derived later. In the present study, in order to express Liu's approach and to avoid the complexity arising from selecting only the independent stress components, all nine stress components are considered. Furthermore, in the present derivation, a less complicated set of parameters is used. First, we introduce an integrating factor, X^0, such that

$$\frac{\mathrm{d}}{\mathrm{d}t}(X^0\mathbf{s}) = 2GX^0\dot{\mathbf{e}} \tag{24}$$

The above equation easily yields

$$\dot{\mathbf{s}} = 2G\dot{\mathbf{e}} - \frac{\dot{X}^0}{X^0}\mathbf{s} \tag{25}$$

Comparing Equations (25) and (16), one obtains the following scalar differential equation:

$$\frac{\dot{X}^0}{X^0} = 2G\dot{\lambda} \tag{26}$$

DOI: 10.1002/nme

Solving the above equation with the initial condition $X^0(0)=1$ leads to

$$X^0 = \exp(2G\lambda) \tag{27}$$

Now, another integrating factor x^0 is introduced, such that

$$\frac{\mathrm{d}}{\mathrm{d}t}[x^0(\tau_\mathrm{y} - \alpha p)] = -\alpha K x^0 \dot{\varepsilon}_v \tag{28}$$

This yields

$$\dot{p} = K\dot{\varepsilon}_v + \frac{\dot{x}^0}{x^0}\frac{1}{\alpha}(\tau_\mathrm{y} - \alpha p) \tag{29}$$

Comparing Equation (29) with Equation (12), the following relationship can be obtained:

$$\frac{\dot{x}^0}{x^0} = -2\alpha^2 K\dot{\lambda} \tag{30}$$

Solving the above scalar differential equation with the initial condition $x^0(0)=1$, one obtains

$$x^0 = \exp(-2\alpha^2 K\dot{\lambda}) \tag{31}$$

Comparing Equations (27) and (31), it is clear that

$$x^0 = (X^0)^{-\alpha^2 K/G} = (X^0)^{1-H/G} \tag{32}$$

Note that Equations (24) and (28) are valid even when the material behaves elastically ($\dot{\lambda}=0$). Now, a new augmented stress vector $\mathbf{X}$ in the $n+2$ dimensional space is defined as

$$\mathbf{X} := \begin{Bmatrix} \mathbf{X}^s \\ X^p \\ X^0 \end{Bmatrix} = \begin{Bmatrix} \mathbf{X}^s \\ x^0(\tau_\mathrm{y} - \alpha p) \\ X^0 \end{Bmatrix} = X^0 \begin{Bmatrix} \mathbf{s} \\ (X^0)^{-H/G}(\tau_\mathrm{y} - \alpha p) \\ 1 \end{Bmatrix} \tag{33}$$

The yield condition, Equation (4), in this new stress space can be expressed in the following form:

$$\tfrac{1}{2}(\mathbf{X}^s)^\mathrm{T}\mathbf{X}^s - (X^0)^{2H/G}(X^p)^2 = 0 \tag{34}$$

In order to reach the form of Equation (23), taking the scalar product of Equation (25) with $\mathbf{s}$ leads to

$$\dot{X}^0\mathbf{s}^\mathrm{T}\mathbf{s} + X^0\mathbf{s}^\mathrm{T}\dot{\mathbf{s}} = 2GX^0\mathbf{s}^\mathrm{T}\dot{\mathbf{e}} \tag{35}$$

In the plastic phase, the yield function leads to the following equation:

$$\mathbf{s}^\mathrm{T}\mathbf{s} = 2(\tau_\mathrm{y} - \alpha p)^2 = 2[(X^0)^{H/G-1}X^p]^2 \tag{36}$$

Substituting Equations (12) and (20) into the consistency condition, Equation (19), leads to

$$\mathbf{s}^\mathrm{T}\dot{\mathbf{s}} = \frac{-2\alpha KG}{H}(\tau_\mathrm{y} - \alpha p)\dot{\varepsilon}_v + \frac{2\alpha^2 KG}{H}\mathbf{s}^\mathrm{T}\dot{\mathbf{e}} \tag{37}$$

DOI: 10.1002/nme

Combining Equations (35)–(37), the following evolution relation for X^0 is achieved:

$$\dot{X}^0 = \frac{1}{\beta}\left[(\mathbf{X}^s)^{\mathrm{T}}\dot{\mathbf{e}} + \frac{\alpha K}{G}(X^0)^{H/G}\dot{\varepsilon}_v\right] \tag{38}$$

where

$$\beta := \frac{H}{G^2}[(X^0)^{H/G-1}X^p]^2 \tag{39}$$

Now, Equations (24), (28) and (38) can be rewritten in a more compact form as

$$\frac{\mathrm{d}}{\mathrm{d}t}(\mathbf{X}) = \frac{\mathrm{d}}{\mathrm{d}t}\begin{Bmatrix}\mathbf{X}^s\\ x^0(\tau_{\mathrm{y}}-\alpha p)\\ X^0\end{Bmatrix} = \begin{Bmatrix}2GX^0\dot{\mathbf{e}}\\ -\alpha K x^0\dot{\varepsilon}_v\\ \dfrac{1}{\beta}\left[\mathbf{X}^s\dot{\mathbf{e}}^{\mathrm{T}} + \dfrac{\alpha K}{G}(X^0)^{H/G}\dot{\varepsilon}_v\right]\end{Bmatrix} \tag{40}$$

or

$$\dot{\mathbf{X}} = \mathbb{A}\mathbf{X} \tag{41}$$

where A is a control matrix and, in the ON phase, is as follows:

$$\mathbb{A} = \begin{bmatrix}\mathbb{O}_{10\times 10} & 2G\left[\dot{\mathbf{e}}, -\dfrac{\alpha K}{2G}(X^0)^{-H/G}\dot{\varepsilon}_v\right]^{\mathrm{T}}\\ \dfrac{1}{\beta}\left[\dot{\mathbf{e}}, \dfrac{\alpha K}{G}(X^0)^{H/G}\dot{\varepsilon}_v\right] & 0\end{bmatrix} \tag{42}$$

Obviously, in the OFF phase, $\dot{X}^0 = 0$ and

$$\mathbb{A} = \begin{bmatrix}\mathbb{O}_{10\times 10} & 2G\left[\dot{\mathbf{e}}, -\dfrac{\alpha K}{2G}(X^0)^{-H/G}\dot{\varepsilon}_v\right]^{\mathrm{T}}\\ \mathbf{0}_{1\times 10} & 0\end{bmatrix} \tag{43}$$

Therefore, the basic plasticity model has been converted into a new model. Since $\mathbb{A}$ is a function of X^0 and X^p, the dynamical system, Equation (41), does not have a closed-form solution. But if one *assumes* that X^0 and X^p are constant in a time interval, $\mathbb{A}$ will depend only on $\dot{\mathbf{e}}$ and $\dot{\varepsilon}_v$. This means that if the strain path is rectilinear, i.e. $\dot{\mathbf{e}}$ and $\dot{\varepsilon}_v$ are constant in each time step, then $\mathbb{A}$ will be constant in each step and there will exist a closed-form solution for Equation (41).

4. EXPLICIT STRESS UPDATING (ALGORITHM I)

A specified strain-controlled path can be approximated by a rectilinear strain path, such that $\dot{\mathbf{e}}$ and $\dot{\varepsilon}_v$ are constant within each time step. These constant values at a discrete time $t = t_n$ are denoted by $\Delta\mathbf{e}_n$ and $\Delta\varepsilon_{v_n}$. Three constitutive quantities, $\boldsymbol{\sigma}_n, \boldsymbol{\varepsilon}_n$ and λ_n, are known at time t_n in a conventional finite element analysis. The updated strains, $\mathbf{e}_{n+1}$ and $\varepsilon_{v_{n+1}}$, are known at t_{n+1}. The stress updating algorithm must integrate the plasticity constitutive equations over each time

DOI: 10.1002/nme

increment to determine $\boldsymbol{\sigma}_{n+1}$ and λ_{n+1}. Here, this is done by solving the dynamical system, Equation (41), with the following initial value:

$$\mathbf{X}_0 = \begin{Bmatrix} \mathbf{X}_0^s \\ X_0^p \\ X_0^0 \end{Bmatrix} = \begin{Bmatrix} \mathbf{s}_0 \\ \tau_y - \alpha p_0 \\ 1 \end{Bmatrix} \tag{44}$$

where $\mathbf{s}_0$ and p_0 are the initial deviatoric stress and initial hydrostatic stress, respectively. It should be mentioned that according to Equation (27), at time $t=0$, constitutive parameter λ is zero and therefore $X^0 = 1$. The solution of Equation (41) is available in the following manner (see Appendix A) for explanations):

$$\mathbf{X}_{n+1} = \exp(\mathbb{A}\Delta t)\mathbf{X}_n \tag{45}$$

As mentioned before, integrating factors X^0 and X^p, which appear in $\mathbb{A}$, are not constants, therefore, $\mathbb{A}$ varies with time in the ON phase. However, X^0 and X^p and therefore $\mathbb{A}$ may be *assumed* constant within each time step. In a fully explicit manner, as suggested by Liu [10], the value of $\mathbb{A}$ at the beginning of each time step, $\mathbb{A}_n$, is considered throughout that step. Therefore, Equation (45) can be expressed as

$$\mathbf{X}_{n+1} = \exp(\mathbb{A}_n\Delta t)\mathbf{X}_n = \mathbb{G}_n\mathbf{X}_n \tag{46}$$

where

$$\mathbb{G}_n = \begin{bmatrix} \mathbb{I}_{10\times 10} + \dfrac{a_n - 1}{c_n^2}\mathbf{A}_{12}\mathbf{A}_{21} & \dfrac{b_n}{c_n}\mathbf{A}_{12} \\ \dfrac{b_n}{c_n}\mathbf{A}_{21} & a_n \end{bmatrix} \tag{47}$$

and

$$\begin{aligned} \mathbf{A}_{12} &= 2G \begin{Bmatrix} \Delta\mathbf{e}_n \\ -\dfrac{\alpha K}{2G}(X_n^0)^{-H/G}\Delta\varepsilon_{v_n} \end{Bmatrix} \\ \mathbf{A}_{21} &= \frac{1}{\beta_n}\left[(\Delta\mathbf{e}_n)^{\mathrm{T}},\ \frac{\alpha K}{G}(X_n^0)^{H/G}\Delta\varepsilon_{v_n}\right] \\ \beta_n &= \frac{H}{G^2}[(X_n^0)^{H/G-1}X_n^p]^2 \\ c_n &= \sqrt{\frac{2G}{\beta_n}(1 - V_n^2)}\|\Delta\mathbf{e}_n\| \\ V_n &= \frac{\alpha K}{G}\frac{\Delta\varepsilon_{v_n}}{\sqrt{2}\|\Delta\mathbf{e}_n\|} \\ a_n &= \cosh(c_n), \quad b_n = \sinh(c_n) \end{aligned} \tag{48}$$

In the above relationships, $\mathbb{I}_{10\times 10}$ is the identity matrix and V_n is a parameter to characterize the ratio of dilatational and deviatoric deformations in the nth time step. Also, it is supposed that

DOI: 10.1002/nme

the nth step is fully plastic and that $\mathbf{s}_n$ lies on the yield surface. Otherwise, similar to all explicit integration schemes, a partially plastic step should be divided into elastic and plastic portions and then contact stress could be determined, e.g. References [6–8]. To accomplish this task, a scalar parameter, r, that divides $\Delta\boldsymbol{\varepsilon}$ into an elastic step, $r\Delta\boldsymbol{\varepsilon}$, and a plastic step, $(1-r)\Delta\boldsymbol{\varepsilon}$, is used. Then, $\Delta\mathbf{e}_n$ and $\Delta\varepsilon_{v_n}$ should be replaced by $(1-r)\Delta\mathbf{e}_n$ and $(1-r)\Delta\varepsilon_{v_n}$ (Equation (48)). Appendix B explains the procedure to calculate r and the corresponding contact stress. In the special case of $V_n = 1$, after addressing the singularity issue, $\mathbb{G}_n$ will have the following form:

$$\mathbb{G}_n = \begin{bmatrix} \mathbb{I}_{10\times 10} + \frac{1}{2}\mathbf{A}_{12}\mathbf{A}_{21} & \mathbf{A}_{12} \\ \mathbf{A}_{21} & 1 \end{bmatrix} \tag{49}$$

Since X^0 and X^p are considered constant in each time step, the induced approximation causes the consistency condition not to be exactly enforced. A remedy to this could be a projection of the solution on the yield surface at the end of each time step. Imposing consistency condition, Equation (34), on the numerical solution of $\mathbf{X}_{n+1}$ leads to

$$X^0_{n+1} = \left[\frac{1}{\sqrt{2}} \frac{\|\mathbf{X}^s_{n+1}\|}{X^p_{n+1}} \right]^{G/H} \tag{50}$$

where $\mathbf{X}^s_{n+1}$ and X^p_{n+1} are computed using Equation (46). Finally, the deviatoric stress at the end of the time step is computed as

$$\mathbf{s}_{n+1} = \frac{\mathbf{X}^s_{n+1}}{X^0_{n+1}} \tag{51}$$

The corresponding mean stress, p_{n+1}, is simply derived from Equation (4). It must be mentioned that X^0 is not a history variable and can be set equal to 1 at the start of each time step.

5. AUGMENTED DIFFERENTIAL EQUATION SYSTEM (ALGORITHM II)

A different scheme proposed by Liu [10] converts the differential Equations (12) and (16) into the following dynamical systems:

$$\begin{aligned} \dot{\mathbf{X}}_a &= \mathbb{A}_a \mathbf{X}_a \\ \dot{\mathbf{X}}_b &= \mathbb{A}_b \mathbf{X}_b \end{aligned} \tag{52}$$

where $\mathbf{X}_a$ and $\mathbf{X}_b$ are augmented stress vectors. These dynamical systems will be solved by an exponential map algorithm. Again, in the present study, to avoid the complexity of Liu's [10] formulation, a different set of parameters is used. Referring to Equation (27), the integrating factor X^0 can be used, such that

$$\frac{\mathrm{d}}{\mathrm{d}t}(X^0\mathbf{s}) = 2GX^0\dot{\mathbf{e}} \tag{53}$$

DOI: 10.1002/nme

Now, a time-dependent scalar parameter, R, which is the radius of the yield surface on the deviatoric plane, is introduced by the following two definitions:

$$\begin{aligned} &\text{(a)} \quad R := \|\mathbf{s}\| \\ &\text{(b)} \quad R := \sqrt{2}(\tau_y - \alpha p) \end{aligned} \tag{54}$$

Taking the scalar product of Equation (53) by $\mathbf{s}$ leads to

$$\dot{X}^0 \mathbf{s}^T \mathbf{s} + X^0 \dot{\mathbf{s}}^T \mathbf{s} = 2GX^0 \dot{\mathbf{e}}^T \mathbf{s} \tag{55}$$

Using the definition of R in Equation (54a), one can easily obtain

$$R^2 = \mathbf{s}^T \mathbf{s}, \quad R\dot{R} = \mathbf{s}^T \dot{\mathbf{s}} \tag{56}$$

Substituting the above relationships into Equation (55) leads to the following scalar differential equation:

$$\frac{\mathrm{d}}{\mathrm{d}t}(X^0 R) = \frac{2G}{R} X^0 \dot{\mathbf{e}}^T \mathbf{s} \tag{57}$$

Now, an augmented stress vector $\mathbf{X}_a$ in the $n+1$ dimensional space is defined as

$$\mathbf{X}_a := \begin{Bmatrix} \mathbf{X}_a^s \\ X_a^0 \end{Bmatrix} = X^0 \begin{Bmatrix} \mathbf{s} \\ R \end{Bmatrix} \tag{58}$$

Equations (53) and (57) can be rewritten in a more compact form as follows:

$$\frac{\mathrm{d}}{\mathrm{d}t}(\mathbf{X}_a) = \frac{\mathrm{d}}{\mathrm{d}t} \begin{Bmatrix} X^0 \mathbf{s} \\ X^0 R \end{Bmatrix} = \begin{Bmatrix} 2GX^0 \dot{\mathbf{e}} \\ \dfrac{2G}{R} X^0 \mathbf{s}^T \dot{\mathbf{e}} \end{Bmatrix} \quad \text{or} \quad \dot{\mathbf{X}}_a = \mathbb{A}_a \mathbf{X}_a \tag{59}$$

where $\mathbb{A}_a$ is a control matrix and, in the ON phase, is as follows:

$$\mathbb{A}_a = \frac{2G}{R} \begin{bmatrix} \mathbb{O}_{9\times 9} & \dot{\mathbf{e}} \\ \dot{\mathbf{e}}^T & 0 \end{bmatrix} \tag{60}$$

Similarly, regarding Equation (31), the integrating factor x^0 can be used, such that

$$\frac{\mathrm{d}}{\mathrm{d}t}[x^0(\tau_y - \alpha p)] = -\alpha K x^0 \dot{\varepsilon}_v \tag{61}$$

Note that x^0 and X^0 are related to each other through Equation (32). Taking the product of the above equation by $(\tau_y - \alpha p)$ leads to the following relationship:

$$x^0(\tau_y - \alpha p)\frac{\mathrm{d}}{\mathrm{d}t}(\tau_y - \alpha p) + \dot{x}^0(\tau_y - \alpha p)^2 = -\alpha(\tau_y - \alpha p) K x^0 \dot{\varepsilon}_v \tag{62}$$

By the definition of R from Equation (54b), one can easily obtain

$$R^2 = 2(\tau_y - \alpha p)^2, \quad R\dot{R} = 2(\tau_y - \alpha p)\frac{\mathrm{d}}{\mathrm{d}t}(\tau_y - \alpha p) \tag{63}$$

DOI: 10.1002/nme

Substituting the above relationships in Equation (62) gives the following scalar differential equation:

$$\frac{\mathrm{d}}{\mathrm{d}t}(x^0 R) = -2\alpha \frac{K}{R}(\tau_{\mathrm{y}} - \alpha p) x^0 \dot{\varepsilon}_v \tag{64}$$

Introducing $\mathbf{X}_b$ vector as

$$\mathbf{X}_b := \begin{Bmatrix} X_b^1 \\ X_b^0 \end{Bmatrix} = x^0 \begin{Bmatrix} \tau_{\mathrm{y}} - \alpha p \\ R \end{Bmatrix} \tag{65}$$

one can rewrite Equations (61) and (64) in the following form:

$$\frac{\mathrm{d}}{\mathrm{d}t}(\mathbf{X}_b) = \frac{\mathrm{d}}{\mathrm{d}t} \begin{Bmatrix} x^0(\tau_{\mathrm{y}} - \alpha p) \\ x^0 R \end{Bmatrix} = \begin{Bmatrix} -\alpha K x^0 \dot{\varepsilon}_v \\ -2\alpha \dfrac{K}{R}(\tau_{\mathrm{y}} - \alpha p) x^0 \dot{\varepsilon}_v \end{Bmatrix} \quad \text{or} \quad \dot{\mathbf{X}}_b = \mathbb{A}_b \mathbf{X}_b \tag{66}$$

where $\mathbb{A}_b$ is a control matrix and, in the ON phase, is as follows:

$$\mathbb{A}_b = -\alpha \frac{K}{R} \dot{\varepsilon}_v \begin{bmatrix} 0 & 1 \\ 2 & 0 \end{bmatrix} \tag{67}$$

Thus, the basic plasticity model has been converted to a new one. $\mathbb{A}_a$ and $\mathbb{A}_b$ are functions of R and, therefore, time dependent. As a result, the dynamical systems, Equation (52), do not have closed-form solutions. But if one *assumes* that R is constant in a time interval, $\mathbb{A}_a$ and $\mathbb{A}_b$ will depend only on $\dot{\mathbf{e}}$ and $\dot{\varepsilon}_v$. This means that if the strain path is rectilinear, i.e. $\dot{e}$ and $\dot{\varepsilon}_v$ are constant within each time step, then $\mathbb{A}_a$ and $\mathbb{A}_b$ will be constant throughout that time interval and there will exist closed-form solutions for these systems.

6. EXPLICIT STRESS UPDATING (ALGORITHM II)

As mentioned before, approximating the strain-controlled path by a rectilinear one, $\dot{\mathbf{e}}$ and $\dot{\varepsilon}_v$ in each time step will have constant values of $\Delta\mathbf{e}_n$ and $\Delta\varepsilon_{v_n}$. To integrate the plasticity constitutive equations, the dynamical systems, Equation (52), must be solved using the following initial values:

$$\mathbf{X}_{a,0} = \begin{Bmatrix} \mathbf{X}_{a,0}^s \\ X_{a,0}^0 \end{Bmatrix} = \begin{Bmatrix} \mathbf{s}_0 \\ \|\mathbf{s}_0\| \end{Bmatrix}, \quad \mathbf{X}_{b,0} = \begin{Bmatrix} X_{b,0}^1 \\ X_{b,0}^0 \end{Bmatrix} = (\tau_{\mathrm{y}} - \alpha p_0) \begin{Bmatrix} 1 \\ \sqrt{2} \end{Bmatrix} \tag{68}$$

where $\mathbf{s}_0$ and p_0 are deviatoric and hydrostatic stresses at time $t = 0$. Note that at time $t = 0$ the constitutive parameter λ is equal to zero, and considering Equations (27) and (31) X^0 and x^0 are equal to one. The solution of Equation (59), when $\mathbb{A}_a$ is a constant, is

$$\mathbf{X}_{a,n+1} = \exp(\mathbb{A}_{a,n} \Delta t) \mathbf{X}_{a,n} = \mathbb{G}_{a,n} \mathbf{X}_{a,n} \tag{69}$$

and

$$\mathbb{G}_{a,n} = \begin{bmatrix} \mathbb{I}_{9\times 9} + (g_n - 1)\Delta\hat{\mathbf{e}}_n (\Delta\hat{\mathbf{e}}_n)^{\mathrm{T}} & h_n \Delta\hat{\mathbf{e}}_n \\ h_n \Delta\hat{\mathbf{e}}_n^{\mathrm{T}} & g_n \end{bmatrix} \tag{70}$$

DOI: 10.1002/nme

where $\Delta\hat{\mathbf{e}}_n$ is the unitary direction of $\Delta\mathbf{e}_n$ and scalar variables g_n and h_n are as follows:

$$g_n = \cosh\left(\frac{2G}{R_n}\|\Delta\mathbf{e}_n\|\right), \quad h_n = \sinh\left(\frac{2G}{R_n}\|\Delta\mathbf{e}_n\|\right) \tag{71}$$

By a similar reasoning, the solution of system, Equation (66), can be obtained as

$$\mathbf{X}_{b,n+1} = \exp(\mathbb{A}_{b,n}\Delta t)\mathbf{X}_{b,n} = \mathbb{G}_{b,n}\mathbf{X}_{b,n} \tag{72}$$

with

$$\mathbb{G}_{b,n} = \begin{bmatrix} u_n & \frac{1}{\sqrt{2}}v_n \\ \sqrt{2}v_n & u_n \end{bmatrix} \tag{73}$$

and

$$u_n = \cosh\left(-\sqrt{2}\alpha\frac{K}{R_n}\Delta\varepsilon_{v_n}\right), \quad v_n = \sinh\left(-\sqrt{2}\alpha\frac{K}{R_n}\Delta\varepsilon_{v_n}\right) \tag{74}$$

Similar to algorithm I, if $\mathbf{s}_n$ is inside the yield surface, one must replace $\Delta\mathbf{e}_n$ and $\Delta\varepsilon_{v_n}$ with $(1-r)\Delta\mathbf{e}_n$ and $(1-r)\Delta\varepsilon_{v_n}$. According to Equation (58), in order to determine $\mathbf{s}_{n+1}$, the value of X^0_{n+1} should be determined. At time $t = t_{n+1}$, Equations (58) and (65) lead to

$$\begin{aligned} X^0_{a,n+1} &= X^0_{n+1} \cdot R_{n+1} \\ X^0_{b,n+1} &= x^0_{n+1} \cdot R_{n+1} \end{aligned} \tag{75}$$

Equation (32) and the above relationships give X^0_{n+1} as equation:

$$X^0_{n+1} = \left[\frac{X^0_{a,n+1}}{X^0_{b,n+1}}\right]^{G/H} \tag{76}$$

Finally, deviatoric stress at the end of time step, $\mathbf{s}_{n+1}$, is computed by

$$\mathbf{s}_{n+1} = \frac{\mathbf{X}^s_{a,n+1}}{X^0_{n+1}} \tag{77}$$

Updated mean stress, p_{n+1}, can be simply computed using Equation (4). As mentioned in the previous updating algorithm, here X^0 and x^0 are auxiliary variables and can be set equal to one simultaneously, at the start of each time step.

7. SEMI-IMPLICIT STRESS UPDATING (ALGORITHM I)

In the present study a more efficient stress-updating scheme will be presented. The evolution law presented in Equation (46) is obviously an explicit one, because $\mathbb{G}_n$ is evaluated on the basis of X^0_n and X^p_n, which are computed at time $t = t_n$, i.e. at the start of the time step. In order to increase the accuracy, one can estimate better values for X^0 and X^p and then compute $\mathbb{G}$ using these values.

DOI: 10.1002/nme

It is intended to use the values of X^0 and X^p at time $t=t_{n+\eta}$, with $0<\eta\leqslant 1$, and assume that they remain constant throughout the step. To do this, first $\mathbf{X}_{n+\eta}$ is computed as

$$\mathbf{X}_{n+\eta}=\exp(\mathbb{A}_n\eta\Delta t)\mathbf{X}_n=\mathbb{G}_n^{\eta}\mathbf{X}_n \tag{78}$$

where

$$\mathbb{G}_n^{\eta}=\begin{bmatrix}\mathbb{I}_{10\times 10}+\dfrac{a_\eta-1}{c_n^2}\mathbf{A}_{12}\mathbf{A}_{21} & \dfrac{b_\eta}{c_n}\mathbf{A}_{12}\\ \dfrac{b_\eta}{c_n}\mathbf{A}_{21} & a_\eta\end{bmatrix} \tag{79}$$

and

$$a_\eta=\cosh(\eta c_n),\quad b_\eta=\sinh(\eta c_n) \tag{80}$$

Note that $\mathbf{A}_{12},\mathbf{A}_{21}$ an c_n are still defined by Equation (48). In the special case of $V_n=1$, after addressing the singularity issue, $\mathbb{G}_n^{\eta}$ has the following form:

$$\mathbb{G}_n^{\eta}=\begin{bmatrix}\mathbb{I}_{10\times 10}+\frac{1}{2}\eta^2\mathbf{A}_{12}\mathbf{A}_{21} & \eta\mathbf{A}_{12}\\ \eta\mathbf{A}_{21} & 1\end{bmatrix} \tag{81}$$

To impose the consistency condition on the numerical solution at time $t=t_{n+\eta}$, it is required to modify $X^0_{n+\eta}$ by the following relationship:

$$X^0_{n+\eta}=\left[\frac{1}{\sqrt{2}}\frac{\|\mathbf{X}^s_{n+\eta}\|}{X^p_{n+\eta}}\right]^{G/H} \tag{82}$$

Finally, $\mathbf{X}_{n+1}$ can be computed using Equation (46), but with a modified $\mathbb{G}_n$ that is calculated at time $t=t_{n+\eta}$:

$$\mathbf{X}_{n+1}=\mathbb{G}_{n+\eta}\mathbf{X}_n \tag{83}$$

where $\mathbb{G}_{n+\eta}$ is computed based on $X^0_{n+\eta}$ and $X^p_{n+\eta}$, i.e.

$$\begin{aligned}\beta_{n+\eta}&=\frac{H}{G^2}[(X^0_{n+\eta})^{H/G-1}X^p_{n+\eta}]^2\\ c_n^*&=\sqrt{\frac{2G}{\beta_{n+\eta}}(1-V_n^2)}\|\Delta\mathbf{e}_n\|\\ a_n^*&=\cosh(c_n^*),\quad b_n^*=\sinh(c_n^*)\end{aligned}$$

DOI: 10.1002/nme

$$\mathbf{A}_{12}^{*} = 2G \begin{Bmatrix} \Delta\mathbf{e}_n \\ -\dfrac{\alpha K}{2G}(X_{n+\eta}^{0})^{-H/G}\Delta\varepsilon_{v_n} \end{Bmatrix}$$
$$\mathbf{A}_{21}^{*} = \frac{1}{\beta_{n+\eta}} \left[(\Delta\mathbf{e}_n)^{\mathrm{T}},\ \frac{\alpha K}{G}(X_{n+\eta}^{0})^{H/G}\Delta\varepsilon_{v_n} \right] \tag{84}$$
$$\mathbb{G}_{n+\eta} = \begin{bmatrix} \mathbb{I}_{10\times 10} + \dfrac{a_n^{*}-1}{(c_n^{*})^2}\mathbf{A}_{12}^{*}\mathbf{A}_{21}^{*} & \dfrac{b_n^{*}}{c_n^{*}}\mathbf{A}_{12}^{*} \\ \dfrac{b_n^{*}}{c_n^{*}}\mathbf{A}_{21}^{*} & a_n^{*} \end{bmatrix}$$

This new scheme is named *semi-implicit*, because an iterative process is not performed to find the converged values of X^0 and X^p at time $t = t_{n+\eta}$.

8. SEMI-IMPLICIT STRESS UPDATING (ALGORITHM II)

This section intends to increase the accuracy of stress-updating algorithm II using a semi-implicit process. According to the definitions of $\mathbb{G}_{a,n}$ and $\mathbb{G}_{b,n}$ in Equations (70) and (73), it is clear that they are computed based on the value of R_n, which is the radius of the yield surface at time $t = t_n$. To develop an implicit method, the two control matrices must be calculated based on the value of $R_{n+\eta}$, which is the radius of the yield surface at time $t = t_{n+\eta}$. First, $X_{a,n+\eta}^{0}$ and $X_{b,n+\eta}^{0}$ are computed using Equations (69) and (72) as

$$X_{a,n+\eta}^{0} = X_n^{0}(h_\eta \mathbf{s}_n^{\mathrm{T}}\Delta\hat{\mathbf{e}} + g_\eta R_n)$$
$$X_{b,n+\eta}^{0} = x_n^{0} R_n(v_\eta + u_\eta) \tag{85}$$

where

$$g_\eta = \cosh\left(\frac{2G}{R_n}\eta\|\Delta\mathbf{e}_n\|\right), \quad h_\eta = \sinh\left(\frac{2G}{R_n}\eta\|\Delta\mathbf{e}_n\|\right) \tag{86}$$

$$u_\eta = \cosh\left(-\sqrt{2}\alpha\frac{K}{R_n}\eta\Delta\varepsilon_{v_n}\right), \quad v_\eta = \sinh\left(-\sqrt{2}\alpha\frac{K}{R_n}\eta\Delta\varepsilon_{v_n}\right) \tag{87}$$

Then, $X_{n+\eta}^{0}$ can be obtained using Equation (76), and finally $R_{n+\eta}$ can be determined as

$$R_{n+\eta} = X_{a,n+\eta}^{0}\left[\frac{X_{a,n+\eta}^{0}}{X_{b,n+\eta}^{0}}\right]^{-G/H} \tag{88}$$

Now, $\mathbf{X}_{a,n+1}$ and $\mathbf{X}_{b,n+1}$ can be computed by Equations (69) and (72) using the modified control matrices calculated at time $t = t_{n+\eta}$ in the following manner:

$$\mathbf{X}_{a,n+1} = \mathbb{G}_{a,n+\eta}\mathbf{X}_{a,n}$$
$$\mathbf{X}_{b,n+1} = \mathbb{G}_{b,n+\eta}\mathbf{X}_{b,n} \tag{89}$$

DOI: 10.1002/nme

where $\mathbb{G}_{a,n+\eta}$ and $\mathbb{G}_{b,n+\eta}$ are computed based on the value of $R_{n+\eta}$ as

$$\mathbb{G}_{a,n+\eta} = \begin{bmatrix} \mathbb{I}_{9\times 9} + (g_n^* - 1)\Delta\hat{\mathbf{e}}_n(\Delta\hat{\mathbf{e}}_n)^{\mathrm{T}} & h_n^*\Delta\hat{\mathbf{e}}_n \\ h_n^*\Delta\hat{\mathbf{e}}_n^{\mathrm{T}} & g_n^* \end{bmatrix} \tag{90}$$

with

$$g_n^* = \cosh\left(\frac{2G}{R_{n+\eta}}\|\Delta\mathbf{e}_n\|\right), \quad h_n^* = \sinh\left(\frac{2G}{R_{n+\eta}}\|\Delta\mathbf{e}_n\|\right) \tag{91}$$

and

$$\mathbb{G}_{b,n+\eta} = \begin{bmatrix} u_n^* & \frac{1}{\sqrt{2}}v_n^* \\ \sqrt{2}v_n^* & u_n^* \end{bmatrix} \tag{92}$$

with

$$u_n^* = \cosh\left(-\sqrt{2}\alpha\frac{K}{R_{n+\eta}}\Delta\varepsilon_{v_n}\right), \quad v_n^* = \sinh\left(-\sqrt{2}\alpha\frac{K}{R_{n+\eta}}\Delta\varepsilon_{v_n}\right) \tag{93}$$

Similar to the previous section, since an iterative process is not performed to find a converged value for $R_{n+\eta}$, the method is referred to as *semi-implicit* formulation.

9. NUMERICAL PRESENTATIONS

In the literature [10], the accuracy and convergency of explicit stress-updating schemes based on exponential maps for the Drucker–Prager plasticity model were not investigated. Therefore, these two issues for the explicit schemes developed by Liu [10] were examined and then compared with the new presented schemes. For the sake of compactness, the following acronyms are adopted:

- EEX(I)—Exponential map with EXplicit stress updating (algorithm I);
- EEX(II)—Exponential map with EXplicit stress updating (algorithm II);
- EIM(I)—Exponential map with semi-IMplicit stress updating (algorithm I);
- EIM(II)—Exponential map with semi-IMplicit stress updating (algorithm II).

The numerical presentations are divided into two sections. In Section 9.1, iso-error maps are presented for the above techniques to explore the accuracy of the algorithm. To make the comparison, these contours are also provided for the backward Euler's method. In Section 9.2, the accuracy and rate of convergency of the methods are explored through a piecewise stress–strain history with different time steps.

9.1. Error contour plots

Error contour plots were first used in the literature by Krieg and Krieg [12] as a tool to present the accuracy of integration methods in J_2 plasticity. Loret and Prevost [1] extended the idea and used the iso-error maps to show the accuracy of forward and backward Euler's techniques in Drucker–Prager's plasticity. In the present study, error contours are used to compare the accuracy of the backward Euler's method with exponential map schemes for both explicit and semi-implicit

DOI: 10.1002/nme

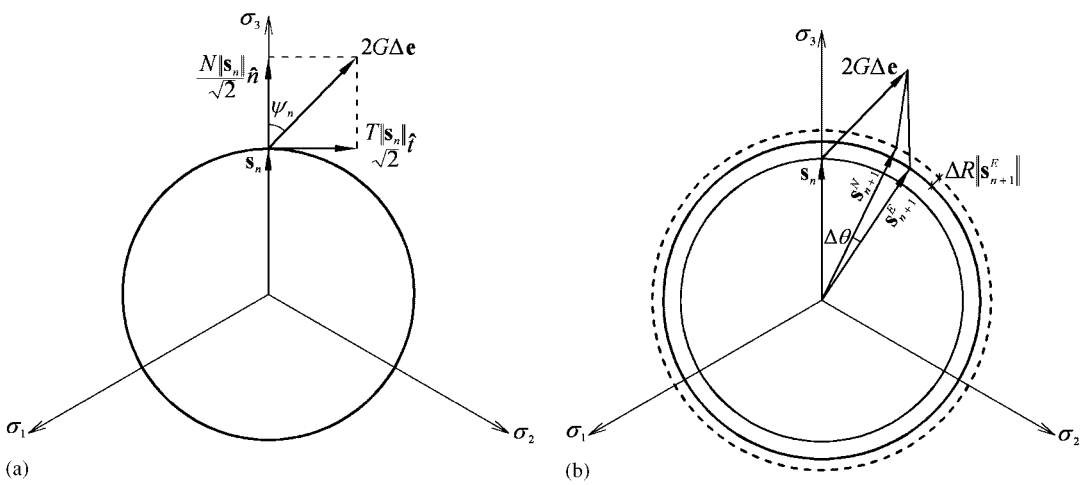

Figure 2. (a) Definition of T, N and ψ_n in the deviatoric plane and (b) definition of a positive $\Delta\theta$ and a negative ΔR.

techniques. The accuracies will be computed for a purely plastic step, which means that the initial stress state, i.e. stress point at time $t = t_n$, lies on the yield surface. Then, an arbitrary deviatoric strain step $\Delta\mathbf{e}$ will be taken with principal directions identical to the principal directions of $\mathbf{s}_n$. Furthermore, a value for V is chosen to completely characterize $\Delta\boldsymbol{\varepsilon}$. Then, stress state at time $t = t_{n+1}$ is computed using a numerical approach and the exact method. In each case, the updated deviatoric stress, $\mathbf{s}_{n+1}$, will have the same principal direction as $\mathbf{s}_n$. This causes the solutions to be conveniently visualized in the deviatoric planes. Now, a parameter that normalizes the deviatoric loading increment is defined as

$$\rho = \frac{2G\|\Delta\mathbf{e}\|}{\|\mathbf{s}_n\|} \tag{94}$$

Then, a reference system of $(\hat{n}, \hat{t})$, which is an orthogonal basis in the deviatoric plane, is selected such that $\hat{n}$ be the unit normal to the loading surface at $\mathbf{s}_n$. A range of prescribed strain rate vectors are examined with the same principal directions as the starting vector. They can be graphically represented in the plane $\hat{n}$–$\hat{t}$ as vectors. Directions of these vectors in the deviatoric plane and their amplitudes can be expressed in terms of a radial and a tangential projection as

$$N = \sqrt{2}\rho\cos(\psi_n), \quad T = \sqrt{2}\rho\sin(\psi_n) \tag{95}$$

As shown in Figure 2(a), ψ_n is the angle between $\Delta\mathbf{e}$ and $\hat{n}$. If one chooses values for the parameters V, N and T, a unique $\Delta\boldsymbol{\varepsilon}$ in principal stress space can be constructed.

Hence, having $\mathbf{s}_n$, p_n and $\Delta\boldsymbol{\varepsilon}$, the deviatoric updated stress vectors $\mathbf{s}^N_{n+1}$ and $\mathbf{s}^E_{n+1}$ can be achieved by numerical and exact methods, respectively. All exact solutions are computed by solving the scalar differential equation extracted by Loret and Prevost [1]. More explanations are offered in Appendix C. Now, the accuracy of a numerical scheme can be fully characterized by the following

DOI: 10.1002/nme

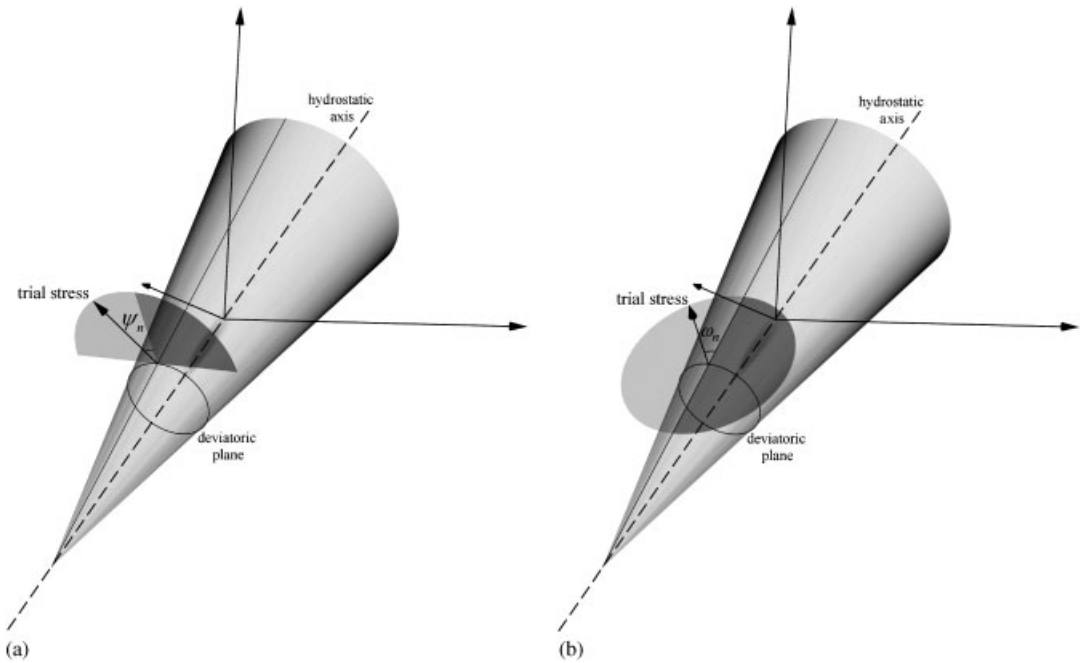

Figure 3. Trial stress vector in stress space: (a) $V=0$ and (b) $V=1$.

two scalar parameters:

$$\Delta\theta = \cos^{-1}\left[\frac{(\mathbf{s}^E_{n+1})^{\mathrm{T}}\mathbf{s}^N_{n+1}}{\|\mathbf{s}^E_{n+1}\|\cdot\|\mathbf{s}^N_{n+1}\|}\right] \tag{96}$$

$$\Delta R = \left[1-\frac{\|\mathbf{s}^N_{n+1}\|}{\|\mathbf{s}^E_{n+1}\|}\right]\times 100\% \tag{97}$$

where $\Delta\theta$ is the error in the orientation of the final deviatoric stress and ΔR describes the relative error in the estimation of the radius of the yield surface in the deviatoric plane. As can be seen in Figure 2(b), the angle $\Delta\theta$ is taken to be positive if $\mathbf{s}^N_{n+1}$ lies between $\mathbf{s}_n$ and $\mathbf{s}^E_{n+1}$. In order to compare the accuracy of different schemes, the iso-error maps are developed for the following N and T domains [1]:

$$-5\leqslant N\leqslant 5, \quad 0\leqslant T\leqslant 5 \tag{98}$$

It is assumed that the material has the following parameters:

$$v=0.125, \quad \alpha=1, \quad \tau_y=0 \tag{99}$$

Two different values for V are selected: $V=0$ and 1. As shown in Figure 3(a), in the case of $V=0$, the trial stress lies on the deviatoric plane and therefore $0\leqslant\psi_n\leqslant\pi/2$ in order to guarantee staying-outside the elastic domain. As a result N can not take a negative value. On the other

DOI: 10.1002/nme

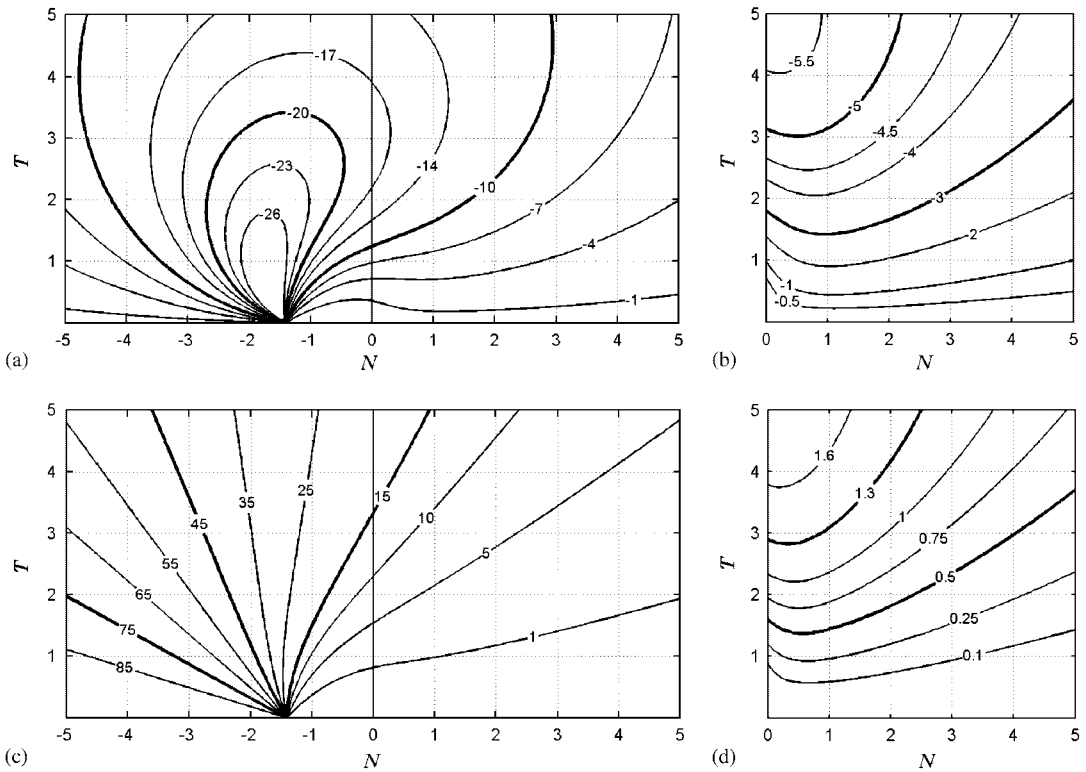

Figure 4. Angular error of Euler's backward method: (a) $V=1$ and (b) $V=0$, and radial error of Euler's backward method: (c) $V=1$ and (d) $V=0$.

hand, in case of $V=1$ as shown in Figure 3(b), the trial stress lies on a plane tangential to the yield surface and does not cross the yield surface, i.e. $0\leqslant\omega_n\leqslant\pi$, which leads to $0\leqslant\psi_n\leqslant\pi$. Note that ψ_n is the projection of ω_n on the deviatoric plane. Therefore, N can take both positive and negative values. Obviously, there is no need to consider negative values for ψ_n due to symmetry and therefore T holds only positive values in both cases. The above conditions are translated as

$$\begin{aligned} V=0: &\quad 0\leqslant N\leqslant 5, \quad 0\leqslant T\leqslant 5 \\ V=1: &\quad -5\leqslant N\leqslant 5, \quad 0\leqslant T\leqslant 5 \end{aligned} \tag{100}$$

Figure 4 shows the angular and radial errors of the one-step backward Euler's method for two different values of V (see Appendix D for a brief explanation of the Euler's method). Figure 5 demonstrates the errors for algorithm I, with an explicit exponential map scheme, i.e. EEX(I). It must be noted that in this method the estimation error for the radius of the yield surface is high for large values of N and T. In other words, the procedure *diverges* as the size of the load step increases. Therefore, a smaller domain, $-0.75\leqslant N\leqslant 0.75$ and $0\leqslant T\leqslant 0.75$, is considered. Figure 6 indicates angular and radial error contours of algorithm II with an explicit exponential map scheme, i.e. EEX(II). As can be seen in this figure, the method has significantly lower error without divergency. Figures 7 and 8 illustrate the iso-error maps for two exponential map methods with semi-implicit

DOI: 10.1002/nme

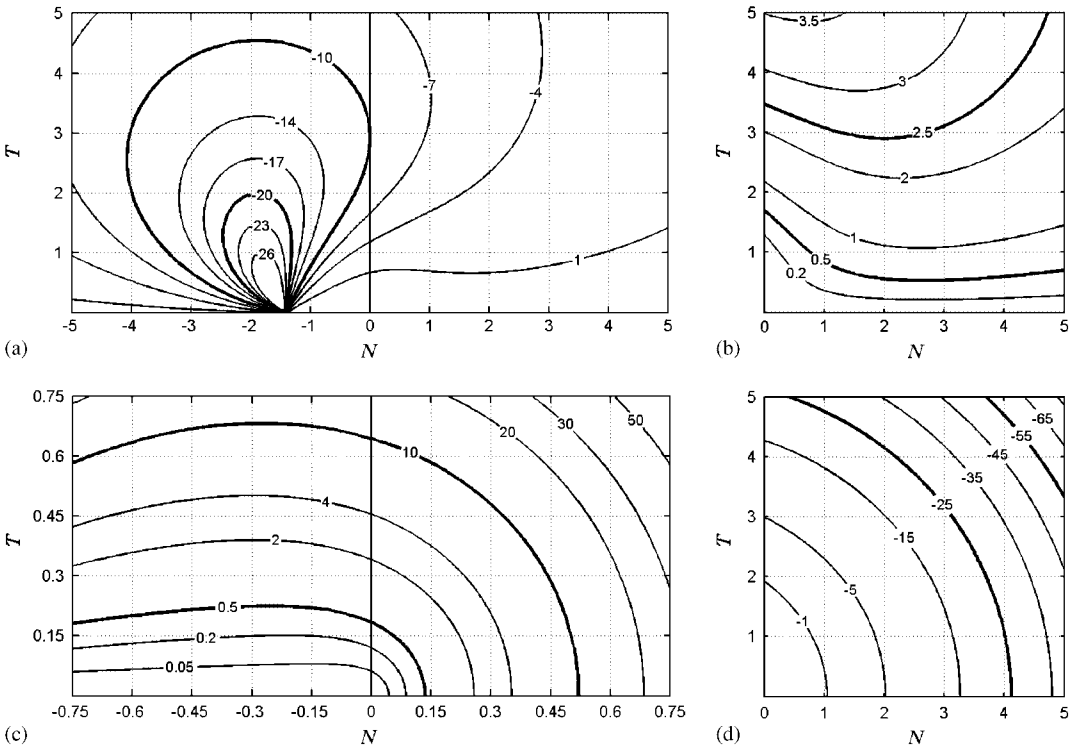

Figure 5. Angular error of EEX(I): (a) $V=1$ and (b) $V=0$, and radial error of EEX(I): (c) $V=1$ and (d) $V=0$.

algorithm, i.e. EIM(I) and EIM(II). Here, a value of 0.5 for the η parameter is chosen, which means that control matrices are computed at the midtime of a load step. These figures reveal the better performance of the EIM(II) method. It seems that all exponential map algorithms show little angular errors, but only semi-implicit ones, especially EIM(II), provide small radial error.

9.2. Pointwise stress–strain test

A biaxial non-proportional strain path is considered. The deviatoric strain component histories are represented graphically in Figure 9. All the other strain components are identically equal to zero. A constant volumetric strain increment is considered through the following relationship:

$$\varepsilon_v(t) = (2 \times 10^{-3}) \cdot t \tag{101}$$

The material is assumed to have the following parameters:

$$\alpha = 0.3, \quad G = 1000\,\text{Mpa}, \quad K = 2167\,\text{Mpa}, \quad \tau_y = 15\,\text{Mpa} \tag{102}$$

It is important to note why a linear strain history is considered. Each integration method operates under the restriction of a constant strain rate vector. For a finite-size load step, this leads to a chordal approximation of a curved strain path. The use of a rectilinear strain path introduces discretization errors. These errors are in addition to the ones from the integration of plasticity rate

DOI: 10.1002/nme

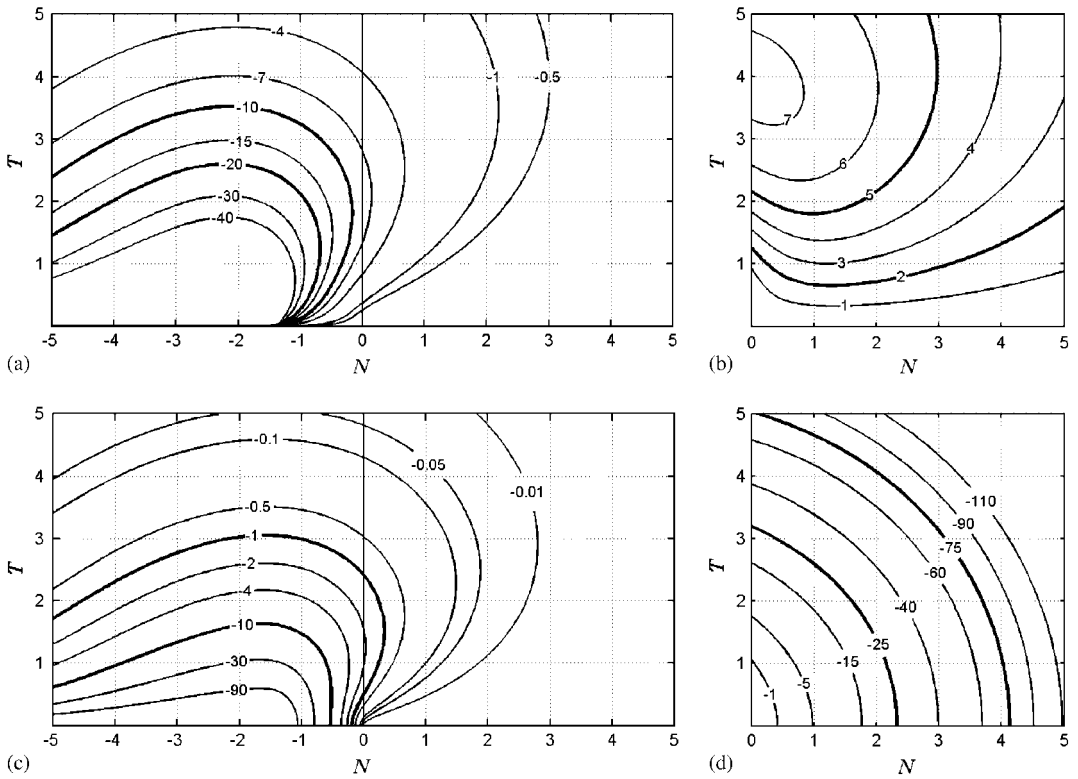

Figure 6. Angular error of EEX(II): (a) $V=1$ and (b) $V=0$, and radial error of EEX(II): (c) $V=1$ and (d) $V=0$.

equations [13]. A linear strain path is chosen to eliminate the discretization errors. To investigate the validity of exponential map algorithms, the results are compared with those of the classical one-step Euler's backward integration (see Appendix D for a brief explanation of the method). The error for the updated deviatoric stress is defined as

$$E_n = \frac{\|\mathbf{s}_n^N - \mathbf{s}_n^E\|}{\|\mathbf{s}_n^E\|} \tag{103}$$

where $\mathbf{s}_n^E$ is the exact updated deviatoric stress vector at time $t=t_n$, and $\mathbf{s}_n^N$ is the numerical one. The exact solution is obtained by solving the scalar differential equation, presented by Loret and Prevost [1], by a fourth-order Runge–Kutta procedure (see Appendix C).

Figure 10 shows the accuracy of Euler's backward method and two EEX schemes. Since the stress relative errors of the EIM formulations are two orders of magnitude smaller than EEX schemes, they are demonstrated separately in Figure 11. In semi-implicit procedures, a value of 0.5 is adopted for η. In this figure, the first few time steps display no error due to the elastic behavior of the material.

To investigate the rate of convergence of the methods, the stress relative error for each scheme is calculated by selecting three practical step sizes of $\Delta t = 0.1, 0.05, 0.025$ s. The results of stress

DOI: 10.1002/nme

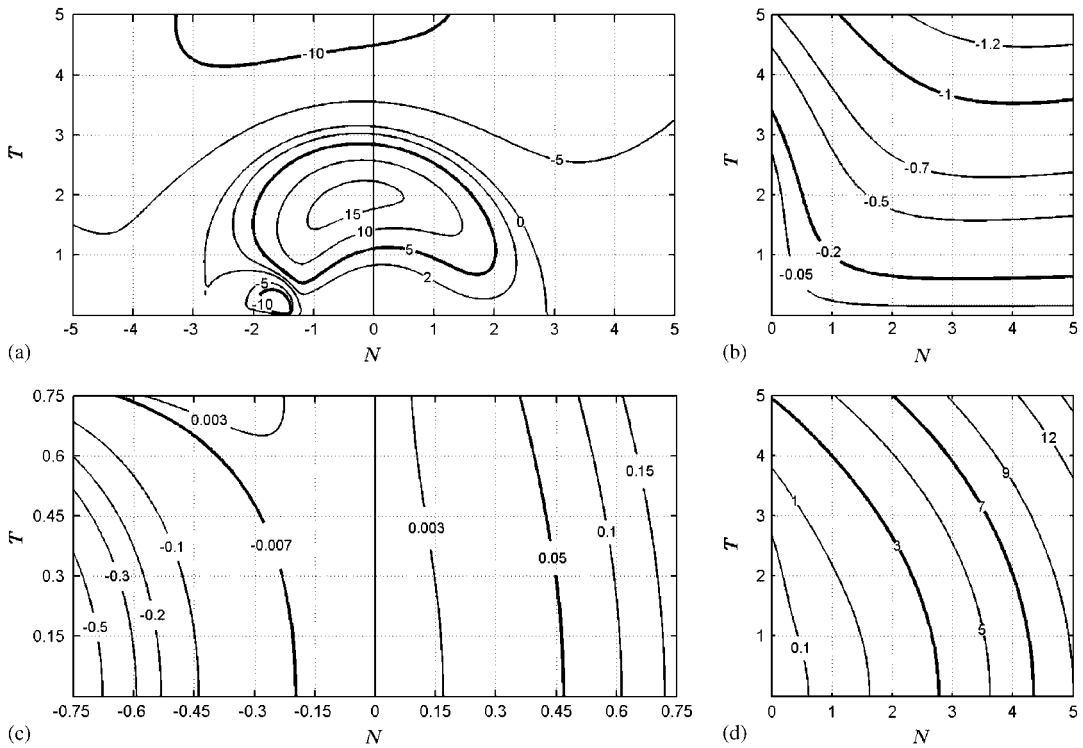

Figure 7. Angular error of EIM(I): (a) $V = 1$ and (b) $V = 0$, and radial error of EIM(I): (c) $V = 1$ and (d) $V = 0$.

relative errors for Euler's backward method, EEX and EIM, are shown in Figures 12–14, respectively. As seen on the figures, EIM formulations have clearly better convergency. Note that using EIM(II) with practical time steps gives a very precise result, which in practical engineering problems may be referred to as a *near-exact* approach.

In order to better investigate the rate of convergence of these methods, here, the *total error* can be defined as [7]

$$E_{\mathrm{T}} = \sum_{n=1}^{N} \Delta t \|\mathbf{s}_n^N - \mathbf{s}_n^E\| \tag{104}$$

where $\mathbf{s}_n^E$ and $\mathbf{s}_n^N$ are defined in Equation (103). Then, by adopting different numbers of substeps, the total error is computed for each scheme. The results are tabulated in Table I and are plotted in Figure 15. In a logarithmic space of Figure 15, the relationship between the total error and the number of sub-steps is linear. The slope of each line represents the rate of convergency of the corresponding method. In the case of Euler's backward scheme, EEX(I) and EEX(II), the slopes represent a linear convergency. In the case of EIM(I) and EIM(II), the quadratic convergency can be clearly appreciated.

DOI: 10.1002/nme

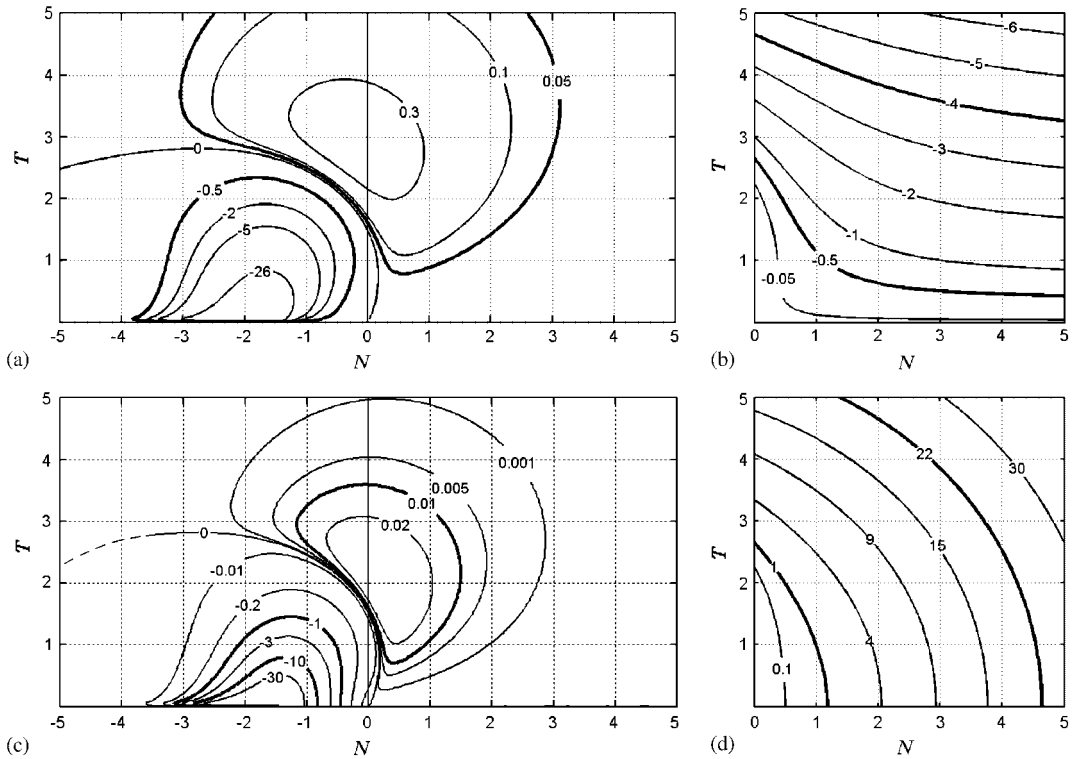

Figure 8. Angular error of EIM(II): (a) $V = 1$ and (b) $V = 0$ and radial error of EIM(II): (c) $V = 1$ and (d) $V = 0$.

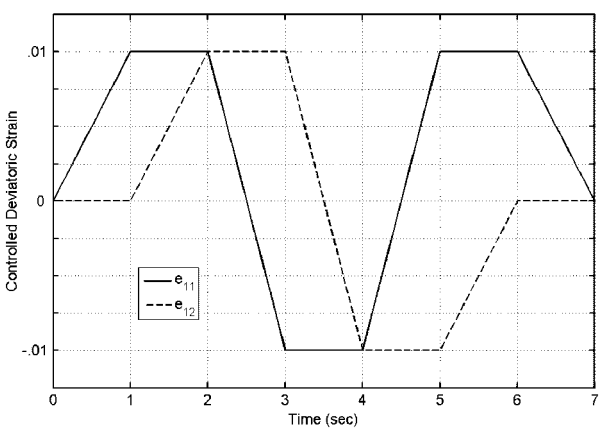

Figure 9. Deviatoric strain component histories.

DOI: 10.1002/nme

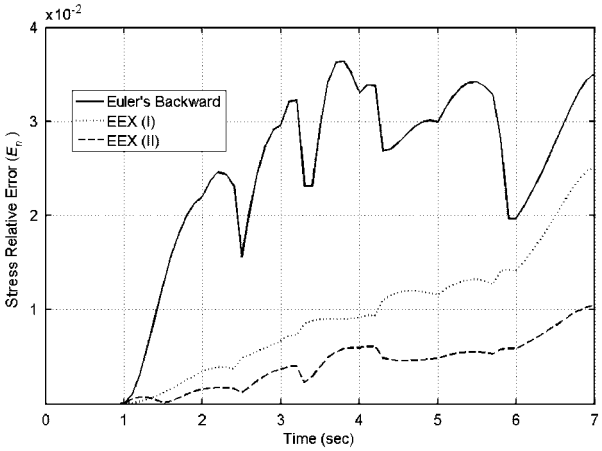

Figure 10. Stress relative error by Euler's backward and two explicit exponential map schemes ($\Delta t = 0.1$ s).

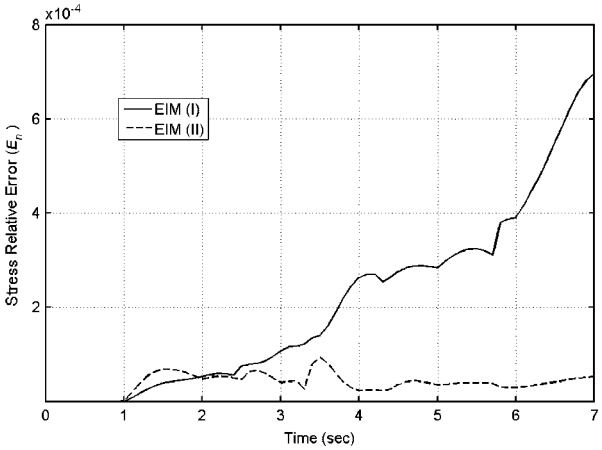

Figure 11. Stress relative error by two implicit exponential map schemes ($\Delta t = 0.1$ s).

10. CONCLUSIONS

Two new numerical schemes based on exponential maps for the solution of the associative Drucker–Prager's elastoplastic constitutive law using a semi-implicit updating algorithm, EIM(I) and (II), are presented. In addition, two previously published methods, referred as EEX(I) and (II) in this study, are discussed and explained for deeper understanding. Extensive numerical tests are performed to compare the performances of all four methods in addition to Euler's backward method. All formulations preserve the consistency condition. Linear convergency of EEX(I) and (II) and quadratic convergency of EIM(I) and (II) are investigated through a pointwise numerical

DOI: 10.1002/nme

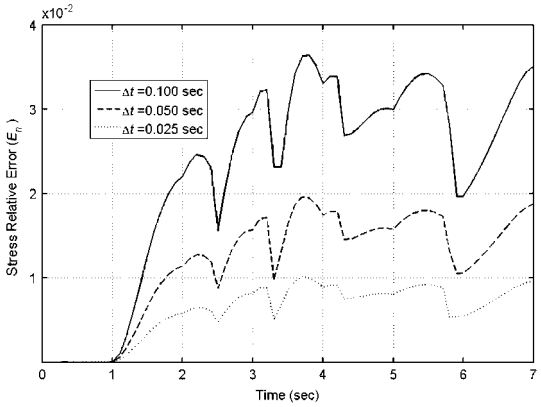

Figure 12. Stress relative error of Euler's backward method with different load step sizes.

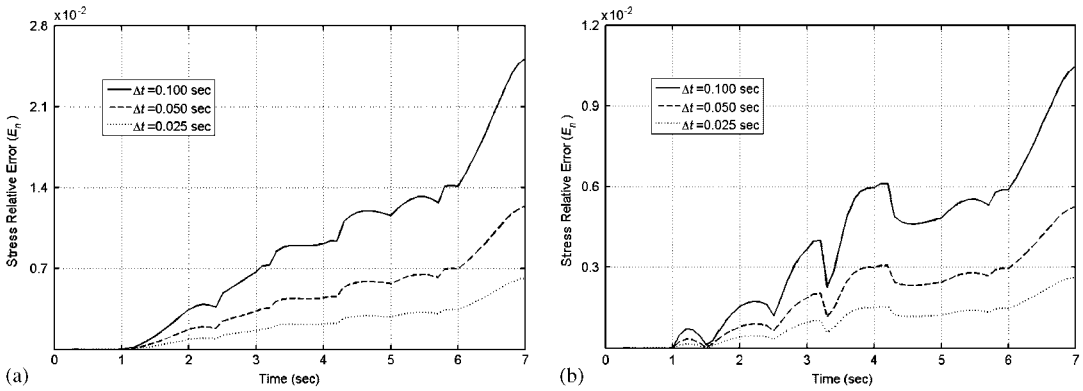

Figure 13. Stress relative error of (a) EEX(I) method and (b) EEX(II) method with different load step sizes.

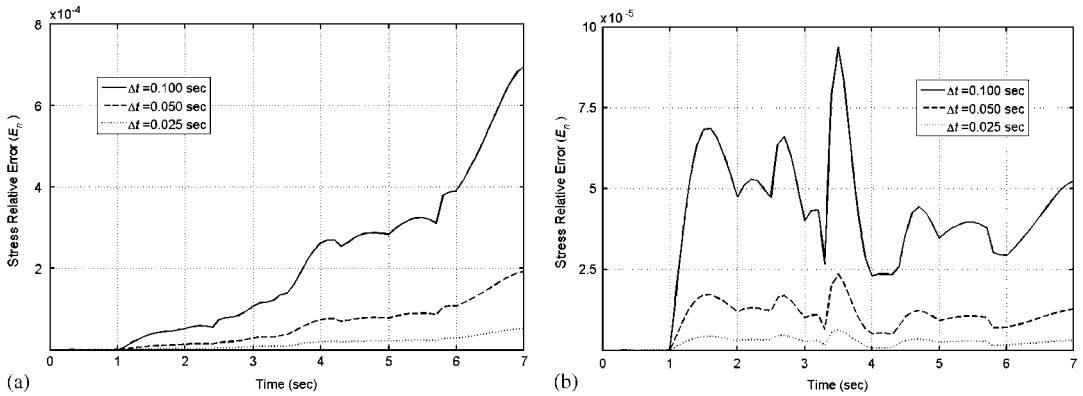

Figure 14. Stress relative error of (a) EIM(I) method and (b) EIM(II) method with different load step sizes.

DOI: 10.1002/nme

Table I. Stress total error for different number of substeps.

No. of substeps	Stress total error (E_T)				
	Euler	EEX(I)	EEX(II)	EIM(I)	EIM(II)
5	46.2747	21.2160	9.3455	0.8515	0.1227
10	25.9949	10.2858	4.8072	0.2613	0.0334
15	17.8923	6.7761	3.2153	0.1234	0.0143
20	13.7394	5.0701	2.4224	0.0729	0.0082
25	11.0632	4.0522	1.9410	0.0480	0.0052
30	9.3081	3.3754	1.6192	0.0343	0.0036
35	8.0110	2.8960	1.3904	0.0258	0.0027
40	7.0455	2.5269	1.2164	0.0202	0.0022

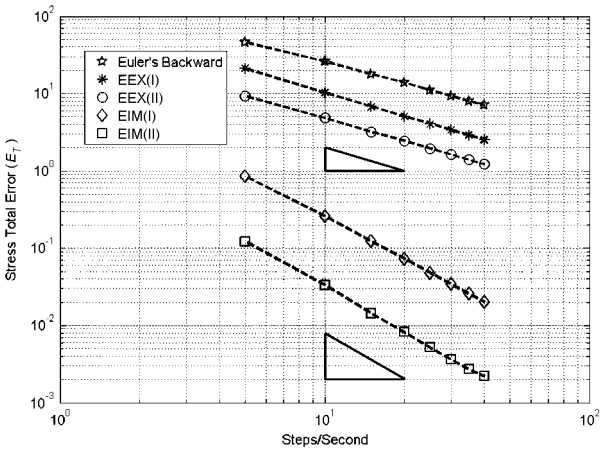

Figure 15. Stress total error *versus* number of substeps.

test. Iso-error maps are presented for all formulations. The important feature arising from these evaluations is that EIM(II) strategy poses the best performance, which may be considered as a near-exact formulation.

APPENDIX A: SOLUTION OF LINEAR DIFFERENTIAL EQUATION SYSTEMS

A system of linear, constant coefficient, ordinary differential equations can be expressed

$$\dot{\mathbf{X}} = \mathbb{A}\mathbf{X} \tag{A1}$$

where $\mathbf{X} = \mathbf{X}(t)$ is a vector function of t, and $\mathbb{A}$ is a matrix independent of t. The solution can be expressed in terms of the matrix exponential

$$\mathbf{X}(t) = \exp(\mathbb{A} \cdot t) \cdot \mathbf{X}(0) \tag{A2}$$

where $\mathbf{X}(0)$ is the initial value of $\mathbf{X}$. When $\mathbb{A}$ is time dependent, one can use a time-discrete variable and *assume* that $\mathbb{A}$ is constant within each time step. Then, using Equation (A2) in a

DOI: 10.1002/nme

successive manner yields

$$\mathbf{X}(t_{n+1}) = \exp(\mathbb{A}_n \cdot \Delta t) \cdot \mathbf{X}(t_n) \tag{A3}$$

Note that the power series which defines the *exponential map* e^x, also defines a map between matrices as

$$\exp(\mathbb{A}) = \mathbb{I} + \mathbb{A} + \frac{\mathbb{A}\mathbb{A}}{2!} + \frac{\mathbb{A}\mathbb{A}\mathbb{A}}{3!} + \cdots \tag{A4}$$

There are mathematical references that explain numerical and analytical methods for computing matrix exponentials, e.g. Golub and Van Loan [14].

APPENDIX B: CALCULATION OF CONTACT STRESS

It is intended to find the scalar parameter r that divides a time step Δt into $r\Delta t$ and $(1-r)\Delta t$, which are a fully elastic and a plastic time step, respectively. Suppose that at time $t = t_n$ the material behaves elastically and stress point is inside the yield surface, which means

$$\tfrac{1}{2}\mathbf{s}_n^{\mathrm{T}}\mathbf{s}_n - (\tau_{\mathrm{y}} - \alpha p_n)^2 < 0 \tag{B1}$$

Now, stress state at the end of time step $r\Delta t$ is calculated using the following elastic relationships:

$$\mathbf{s}_{n+r} = \mathbf{s}_n + 2Gr\Delta\mathbf{e} \tag{B2}$$

$$p_{n+r} = p_n + Kr\Delta\varepsilon_v \tag{B3}$$

It is considered that at the end of time step $r\Delta t$ stress state lies exactly on the yield surface, i.e.

$$\tfrac{1}{2}\mathbf{s}_{n+r}^{\mathrm{T}}\mathbf{s}_{n+r} - (\tau_{\mathrm{y}} - \alpha p_{n+r})^2 = 0 \tag{B4}$$

Substituting Equations (B2) and (B3) into (B4) leads to the following algebraic equation:

$$Ar^2 + Br + C = 0 \tag{B5}$$

where

$$A = 4G^2\Delta\mathbf{e}^{\mathrm{T}}\Delta\mathbf{e} - 2K^2\alpha^2\Delta\varepsilon_v^2 \tag{B6}$$

$$B = 4G\mathbf{s}_n^{\mathrm{T}}\Delta\mathbf{e} + 4K\alpha(\tau_{\mathrm{y}} - \alpha p_n)\Delta\varepsilon_v \tag{B7}$$

$$C = \mathbf{s}_n^{\mathrm{T}}\mathbf{s}_n - 2(\tau_{\mathrm{y}} - \alpha p_n)^2 \tag{B8}$$

Finally, contact stress, $\mathbf{s}_{\mathrm{c}}$, may be computed using an elastic updating

$$\mathbf{s}_{\mathrm{c}} = \mathbf{s}_n + 2Gr\Delta\mathbf{e} \tag{B9}$$

APPENDIX C: EXACT SOLUTIONS

Loret and Prevost [1] presented an exact solution for Drucker–Prager's elastoplastic equations as a part of a comprehensive study. Here, a brief review of their method is presented. Suppose that

DOI: 10.1002/nme

$\mathbf{s}_n$ lies on the yield surface and $\Delta\mathbf{e}_n$ and $\Delta\varepsilon_{v_n}$ are increments of deviatoric and volumetric strains in the nth time step. The heart of the scheme is the following scalar differential equation:

$$\operatorname{sign}(\sin\psi)\cdot\frac{\frac{1}{2}\dot{\psi}}{|\sin\frac{1}{2}\psi|^{p}\cdot|\cos\frac{1}{2}\psi|^{q}}=-\frac{2G\|\Delta\mathbf{e}\|}{\|\mathbf{s}_n\|}\cdot\frac{1}{|\sin\frac{1}{2}\psi_n|^{p-1}\cdot|\cos\frac{1}{2}\psi_n|^{q-1}} \tag{C1}$$

where exponents p and q are defined as

$$p=2-\frac{G}{H}(1+V_n),\quad q=2-\frac{G}{H}(1-V_n) \tag{C2}$$

V_n and H are defined in Equations (48) and (21), respectively. ψ_n, the angle between $\Delta\mathbf{e}$ and $\mathbf{s}_n$, is presented graphically in Figure 2(a) and can be computed by

$$\psi_n=\cos^{-1}\left(\frac{\mathbf{s}_n^{\mathrm{T}}\Delta\mathbf{e}}{\|\mathbf{s}_n\|\cdot\|\Delta\mathbf{e}\|}\right) \tag{C3}$$

As p and q in Equation (C1) are not usually integers, this equation does not have a closed-form solution. Using an accurate Runge–Kutta procedure in [0, 1] interval, Equation (C1) may be integrated numerically to find $\psi_{n+1}=\psi(1)$. Finally, the updated deviatoric stress can be obtained using the following relationships:

$$\begin{aligned}\mathbf{s}_{n+1}&=P(\mathbf{s}_n+2GQ\Delta\mathbf{e})\\ P&=\frac{\|\mathbf{s}_{n+1}\|\sin\psi_{n+1}}{\|\mathbf{s}_n\|\sin\psi_n},\quad Q=\frac{\|\mathbf{s}_n\|\sin(\psi_n-\psi_{n+1})}{2G\|\Delta\mathbf{e}\|\sin\psi_{n+1}}\\ \|\mathbf{s}_{n+1}\|&=\|\mathbf{s}_n\|\left|\frac{\sin\frac{1}{2}\psi_{n+1}}{\sin\frac{1}{2}\psi_n}\right|^{1-p}\left|\frac{\cos\frac{1}{2}\psi_{n+1}}{\cos\frac{1}{2}\psi_n}\right|^{1-q}\end{aligned} \tag{C4}$$

Obviously, if $\mathbf{s}_n$ is inside the yield surface, contact stress must be determined through calculating a scalar parameter r, which is explained in Appendix B. Loret and Prevost [1] presented some remarks on the method and discussed about the cases in which singularity arises in Equation (C1). As they claimed, this method is very time consuming. In the present study, the above-mentioned method is used as a benchmark for the proposed numerical techniques.

APPENDIX D: EULER'S BACKWARD METHOD

It is intended to briefly show how constitutive equations are integrated by the one-step backward Euler integration method. Assume that the stress vector $\boldsymbol{\sigma}_n$ at time $t=t_n$ and the strain vector increment $\Delta\boldsymbol{\varepsilon}$ are known. Decomposing $\Delta\boldsymbol{\varepsilon}$ into deviatoric and volumetric parts, a trial elastic stress vector is established. Its deviatoric and volumetric components are as follows:

$$\begin{aligned}\mathbf{s}_{n+1}^{\mathrm{tr}}&=\mathbf{s}_n+2G\Delta\mathbf{e}\\ p_{n+1}^{\mathrm{tr}}&=p_n+K\Delta\varepsilon_v\end{aligned} \tag{D1}$$

DOI: 10.1002/nme

It may be shown that updated deviatoric stress vector and volumetric stress at the end of a time step can be obtained as

$$\mathbf{s}_{n+1} = \mathbf{s}^{\mathrm{tr}}_{n+1} - \lambda G\sqrt{2}\frac{\mathbf{s}^{\mathrm{tr}}_{n+1}}{\|\mathbf{s}^{\mathrm{tr}}_{n+1}\|} \tag{D2}$$

$$p_{n+1} = p^{\mathrm{tr}}_{n+1} - \lambda K\alpha \tag{D3}$$

where

$$\lambda = \frac{f(\boldsymbol{\sigma}^{\mathrm{tr}}_{n+1})}{G + \alpha^2 K} \tag{D4}$$

In Equation (D4), f is the yield function defined in Equation (3). Equation (D2) shows that the deviatoric plastic strain vector is assumed to lie parallel to the trial deviatoric stress vector. In other words, the final stress is found through a radial return in deviatoric plane accompanied by a change in mean stress. In this method, $\boldsymbol{\sigma}_n$ may be inside the yield surface and there is no need to find the contact stress.

REFERENCES

1. Loret B, Prevost JH. Accurate numerical solutions for Drucker–Prager elastic–plastic models. *Computer Methods in Applied Mechanical Engineering* 1986; **54**:259–277.
2. Genna F, Pandolfi A. Accurate numerical integration of Drucker–Prager's constitutive equations. *Meccanica* 1994; **29**:239–260.
3. Hong H-K, Liu C-S. Internal symmetry in the constitutive model of perfect elastoplasticity. *International Journal of Non-Linear Mechanics* 2000; **35**:447–466.
4. Hong H-K, Liu C-S. Internal symmetry in bilinear elastoplasticity. *International Journal of Non-Linear Mechanics* 1999; **34**:279–288.
5. Liu C-S. Symmetry groups and the pseudo-Riemann spacetimes for mixed-hardening elastoplasticity. *International Journal of Solids and Structures* 2003; **40**:251–269.
6. Auricchio F, Beirão da Veiga L. On a new integration scheme for von-Mises plasticity with linear hardening. *International Journal for Numerical Methods in Engineering* 2003; **56**:1375–1396.
7. Artioli E, Auricchio F, Beirão da Veiga LB. Integration schemes for von-Mises plasticity models based on exponential maps: numerical investigations and theoretical considerations. *International Journal for Numerical Methods in Engineering* 2005; **64**:1133–1165.
8. Artioli E, Auricchio F, Beirão da Veiga LB. A novel 'optimal' exponential-based integration algorithm for von-Mises plasticity with linear hardening: theoretical analysis on yield consistency, accuracy, convergence and numerical investigations. *International Journal for Numerical Methods in Engineering* 2006; **4**:449–498.
9. Rezaiee-Pajand M, Nasirai C. Accurate integration scheme for von-Mises plasticity with mixed-hardening based on exponential maps. *Engineering Computations* 2007; **24**(6):608–635.
10. Liu C-S. Internal symmetry groups for the Drucker–Prager material model of plasticity and numerical integrating methods. *International Journal of Solids and Structures* 2004; **41**:3771–3791.
11. Chen WF, Han DJ. *Plasticity for Structural Engineers*. Springer: New York, 1988.
12. Krieg RD, Krieg DB. Accuracies of numerical solution methods for elastic-perfectly plastic model. *Journal of Pressure Vessel Technology*, *Transaction of the ASME* 1977; **99**:510–515.
13. Dodds RH. Numerical techniques for plasticity computations in finite element analysis. *Computers and Structures* 1987; **26**(5):767–779.
14. Golub GH, Van Loan CF. *Matrix Computation*. Johns Hopkins University Press: Baltimore, MD, 1983.

DOI: 10.1002/nme